Molecular Electronics

DOI: 10.1002/ange.201306953

Growth of Ultrathin Organic Semiconductor Microstripes with Thickness Control in the Monolayer Precision**

Liqiang Li, Peng Gao, Wenchong Wang, Klaus Müllen, Harald Fuchs, and Lifeng Chi**

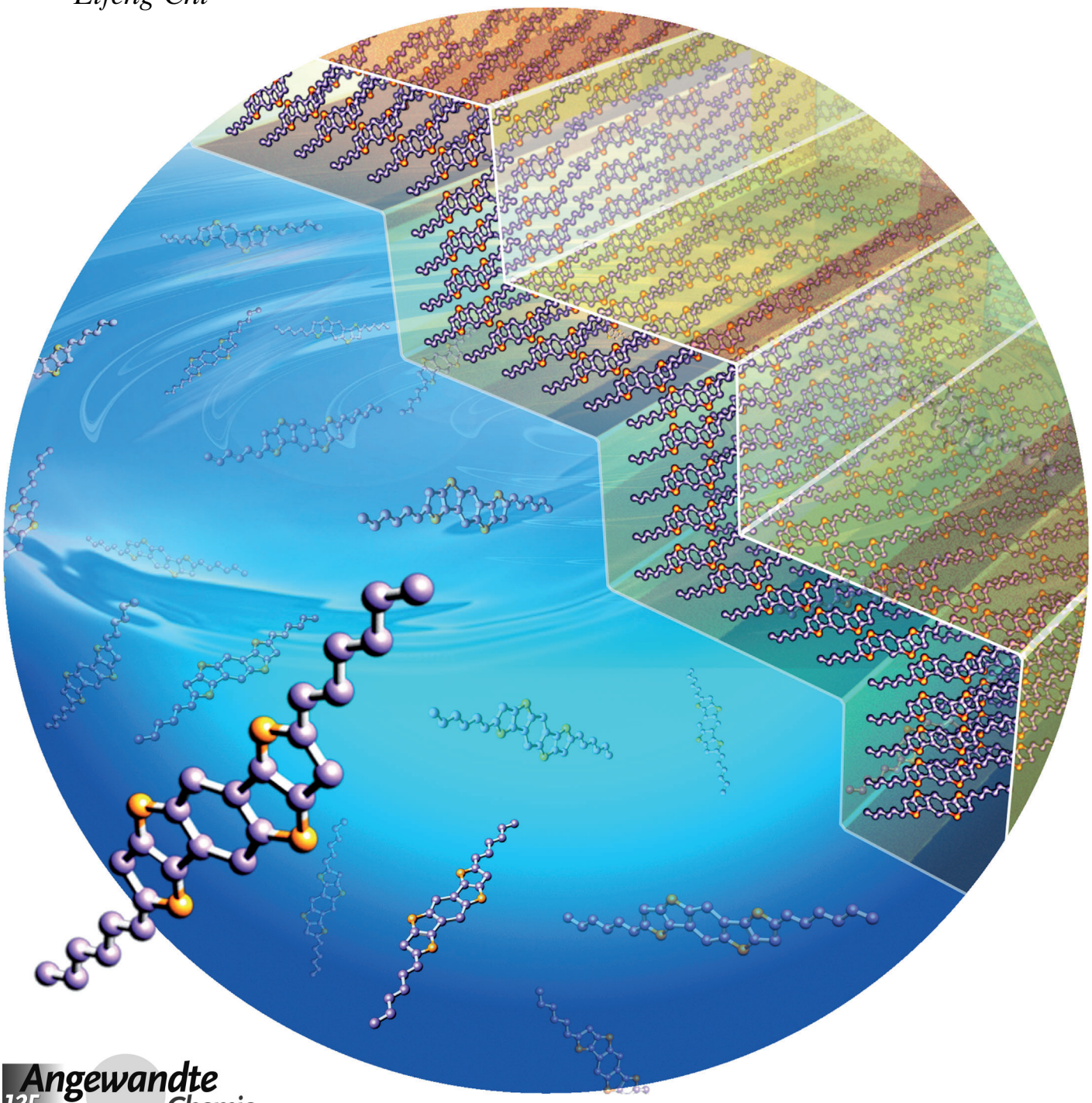

Control over the growth or assembly of organic semiconductors (OSCs) is of great significance for organic electronics.[1–3] Monolayer precision growth of continuous, uniform, microstructured OSC films in nanometer thickness range ($\leq$15 nm) may provide elaborate systems for some fundamental research and device applications such as sensors.[4] However, until now, it is quite challenging to grow OSC films that simultaneously satisfy the above-mentioned four features (nanometer thickness, monolayer precision, thickness uniformity over large area, and microstructuring with at least 1D continuity) because of the great compromise of these features.

Currently, nanometer films of pristine OSCs have been obtained by Langmuir–Blodgett (LB) and Langmuir–Schäfer (LS) vacuum deposition, drop casting, and spin coating.[4,5] However, these methods generally produce discontinuous ultrathin patches or continuous terrace islands with grain boundaries, which means imperfect lateral continuity and thickness uniformity. Furthermore, the thickness control precision of these methods is normally an average value which is not real a monolayer precision.

Here we demonstrate the monolayer precision growth of uniform monolayer to hexalayer (about 1.6–12 nm) dendritic OSC microstripes (a kind of microstructured film) over large areas using a dip-coating process. The pulling speed has a great impact on the molecular layer number and the thickness uniformity. At low-speed regime, the layer number decreases with increased pulling speed, and the microstripes with different layer number are mixed together, which is coincident with our previous work.[6] When the pulling speed is higher than the transition value, the layer number is generally proportional to the pulling speed. Remarkably, in this regime, uniform monolayer to hexalayer microstripes can be obtained with perfect monolayer precision over a large area. Although monolayer precision may be achieved by other methods such as LB technique, which is however generally restricted to amphiphilic molecules and thus may compromise the electrical property.

Figure 1 b–g shows the $50\times50\ \mu m^2$ AFM images and section profiles of monolayer to hexalayer microstripes of DTBDT-C6 (Figure 1 a) obtained at high pulling speed

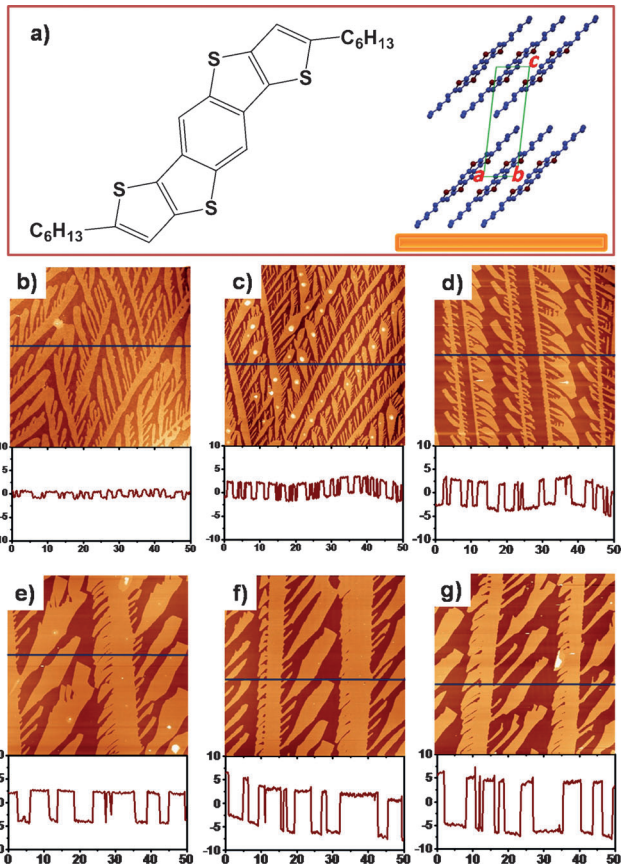

Figure 1. a) Molecular structure of DTBDT-C6 and packing structure in the microstripes. AFM image ($50\times50\ \mu m^2$) and section profile of b) monolayer microstripes at $U=200\ \mu m\,s^{-1}$, c) bilayer microstripes at $U=1000\ \mu m\,s^{-1}$, d) trilayer microstripes at $U=2000\ \mu m\,s^{-1}$, e) tetralayer microstripes at $U=3000\ \mu m\,s^{-1}$, f) pentalayer microstripes at $U=10000\ \mu m\,s^{-1}$, and g) hexalayer microstripes at $U=10000\ \mu m\,s^{-1}$. The solution concentration for all the experiments is 2 mg mL^{-1}. The unit for the *x* and *y* axes in the section profile is micrometer and nanometer, respectively.

($>50\ \mu m\,s^{-1}$), which clearly denote the uniformity of the microstripes. The height of a monolayer ($d1$) is about 1.65-1.75 nm. The corresponding value of multilayers (dn) fits well the equation $dn = N\times d1$, where N is the molecular layer number. XRD measurements (Figure S1) on multilayer ($N\geq2$) microstripes indicate the DTBDT-C6 molecules adopt edge-on orientation on the substrates (Figure 1 a, right part).

During AFM measurements, the AFM tip was moved along the microstripes or to the different locations of the samples to check the uniformity over a large area. In some samples, the uniform monolayer and bilayer microstripes are over centimeter size. The uniform coverage for a trilayer is in the millimeter range, while the domain with pure tetralayer, pentalayer or hexalayer is well-separated and the size of each domain is about hundreds of micrometer. Apart from large-area uniformity, the large-area scanning electron microscopy (SEM; Figure S2) and AFM characterizations also reveal the main trunks of the dendrite are continuous and well aligned over hundreds of micrometers, which means a good continuity along one direction. The 1D continuity, uniformity, and

[*] Dr. L. Q. Li, Dr. W. C. Wang, Prof. H. Fuchs, Prof. L. F. Chi
Physikalisches Institut and Center for Nanotechnology (CeNTech)
Universität Münster, 48149 Münster (Germany)
E-mail: chi@uni-muenster.de
Dr. P. Gao, Prof. K. Müllen
Max Planck Institute for Polymer Research
Ackermannweg 10, 55128 Mainz (Germany)
E-mail: muellen@mpip-mainz.mpg.de
Prof. L. F. Chi
Institute of Functional Nano and Soft Materials (FUNSOM) and Collaborative Innovation Center of Suzhou Science and Technology
Soochow University, 199 Ren-Ai Road, Suzhou Jiangsu 215123 (P.R. China)

[**] This work was funded by the Germany–China Joint Project TRR61 (DFG-NSFC Transregio Project), the NSFC key project (grant number 91227201) and EU project (grant number FP7-People-2009-IRSES/247641).

Supporting information for this article is available on the WWW under http://dx.doi.org/10.1002/anie.201306953.

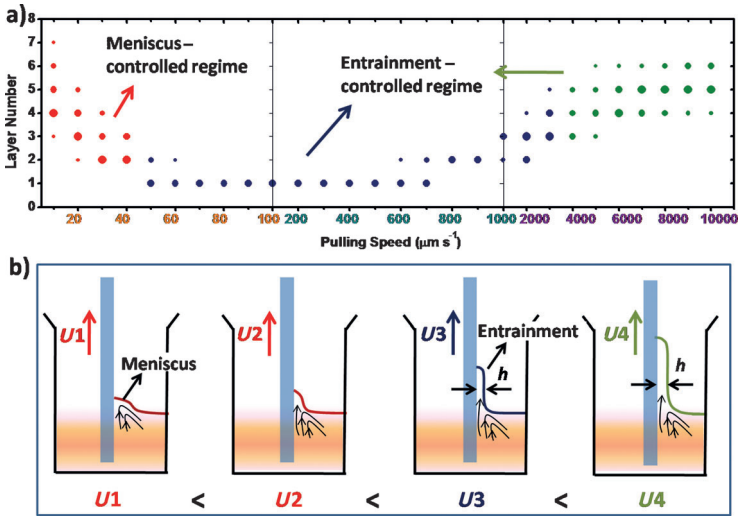

Figure 2. a) The relationship between the molecular layer number and pulling speed for 2 mg mL^{-1} solution. Red symbols indicate that microstripes with different layer numbers are mixed. Blue symbols indicate that microstripes with different layer numbers are well-separated. Green symbol indicate that there are well-separated as well as mixed microstripes. The size of the symbols denotes approximately the distribution of microstripes with each layer. b) The growth mechanism, showing the status and evolution of the three-phase contact area at different pulling speeds of the dip-coating process. *U*1 and *U*2 are within the meniscus-controlled regime, corresponding to the red-symbol regime in (a). *U*3 and *U*4 are within the entrainment-controlled regime, corresponding to the blue- and green-symbol regime in (a), respectively.

alignment over large areas facilitate the fabrication of planar electronic devices.

Figure 2a displays the dependence of molecular layer number (N) on the pulling speed (U) with a solution concentration of 2 mg mL^{-1}. When 10 μm s^{-1} ≤ U ≤ 40 μm s^{-1} (red-symbol regime), N decreases with increasing U, and microstripes with different N are mixed together (Figure S3). At U = 50 and 60 μm s^{-1}, well-separated and uniform monolayer and bilayer microstripes over large area are formed. For 70 μm s^{-1} ≤ U ≤ 500 μm s^{-1}, only monolayer microstripes are obtained nearly over the whole substrates, as shown in Figure S2a and Figure S4. However, the morphology and coverage of monolayer microstripes in this speed regime vary with U (Figure S2a and Figure S4). Once U is higher than 600 μm s^{-1}, N is nearly proportional to U. Remarkably, at 50 μm s^{-1} ≤ U ≤ 3000 μm s^{-1} (blue-symbol regime, Figure 2a), the microstripes with different N are generally well separated from each other, while at 4000 μm s^{-1} ≤ U ≤ 10000 μm s^{-1} (green-symbol regime, Figure 2a), well-separated microstripes as well as mixed microstripes are formed. From Figure 1 and Figures S2–S4, it can be found that the morphology shows dependence on the pulling speed. Theoretical modeling of the formation of such fractal structure is ongoing.

Figure 2a reveals the different N–U relationships (inverse, constant, proportional). The thickness dependence on the pulling speed in the dip-coating process is a common knowledge for film preparation, and two growth regimes (inverse and proportional thickness–pulling speed relationships) were reported for the dip-coating processes of phospholipids, sol-gel systems, and polymers.[7] However, there are two unique progresses of our work compared with the previous ones:[7–9] 1) precise thickness control at molecular level and 2) vertical thickness in the nanometer regime with lateral microstructuring and 1D continuity. A film with those two distinguished characteristics is quite challenging to achieve because of the great compromise between them. In the previous reports the thickness of the coated film is generally over tens of nanometers, and the thickness control precision is an average value (tens of nanometers or more) and far from molecular level. "Real monolayer precision" achieved in this work represents a significant progress compared to "average thickness" reported previously.

Figure 2b shows the growth mechanism in the dip-coating process. When the substrate is immersed into the solution, a meniscus climbs up the substrate. Pulling the substrate out of the solution at low speed U1, a pinned meniscus area rises with the substrates and becomes stretched gradually because of the viscous drag.[7,8] With the rapid evaporation of the solvent near the contact line and continuous supply of solute molecules toward the contact line by convection flow and capillary force, the amount of solute molecules increases and finally nucleation center form at the contact line. The supplied solute aggregates onto the nucleation center and continues to grow into stripes by self-assembly during continuous solvent evaporation and substrate movement. The nonuniform convection flow in the meniscus area brings about the nonuniform concentration distribution of solute molecules, which may result in mixed microstripes with different N. In this speed regime, higher speed (U2) leads to a thinner meniscus and a higher three-phase contact line above the solution surface, and thus less solute molecules accumulate at the contact line.[7,8] This can explain the inverse N–U relationship. Therefore the growth at low U regime (red-symbol regime in Figure 3a) is controlled by the meniscus.

When the pulling speed is higher than the transition value (≈ 50 μm s^{-1} in our case), a uniform liquid thin film is dragged out of the meniscus and entrained onto the substrate (U3 and

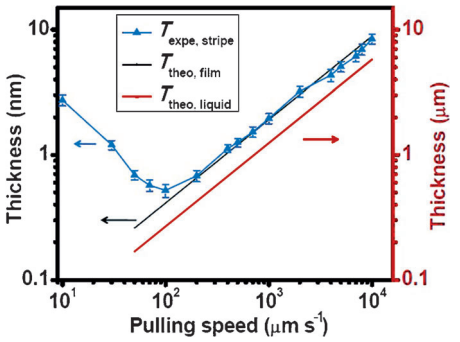

Figure 3. Plots of $T_{expe,stripe}$, $T_{theo,liquid}$, and $T_{theo,film}$ versus the pulling speed. $T_{expe,stripe}$ is the experimental thickness (average value) of microstripes. $T_{theo,liquid}$ is the theoretical thickness of entrained liquid film ($T_{theo,liquid}$). $T_{theo,film}$ is the theoretical thickness of solute film after solvent evaporation.

*U*4 in Figure 2b, and Figure S5).[7,9] The entrained liquid film (referred to as entrainment, see Figure S5) moves with the substrate. The entrainment is quite uniform, and therefore provides an excellent platform for the growth of uniform microstripes over a large area. Generally, the thickness (h) of entrainment on the substrates can be approximately predicted by Landau–Levich equation [Eq. (1)],[9a]

$$h = 0.944(\mu U)^{2/3}/\sigma^{1/6}(\rho g)^{1/2} \quad (1)$$

where ρ, μ, and σ are the density, viscosity, and surface tension of the solution, respectively, and g is the gravity acceleration.

Based on the Landau–Levich equation, the theoretical thickness of an entrained liquid film ($T_{theo,liquid}$) can be approximately calculated. In this calculation, the ρ (866.90 kg m^{-3}), μ (5.5×10^{-4} N s m^{-1}), and σ (2.852×10^{-2} N m^{-1}) of the solvent (toluene) are used for the OSC solution. Then, the theoretical thickness of the solute film ($T_{theo,film}$) after solvent evaporation can be further calculated approximately by $T_{theo,film} = (T_{theo,liquid}\times C)/\rho_{film}$, where C is solution concentration (2 mg mL^{-1}), and ρ_{film} is the density of solute film which is calculated to be about 1.3 g cm^{-3} from the crystal structure. $T_{theo,liquid}$, $T_{theo,film}$, and $T_{expe,stripe}$ (averaged experimental thickness of microstripes) versus U are drawn as red, black, and blue lines in Figure 3, respectively. At $U \geq$ 200 μm s^{-1}, there is a good agreement between $T_{expe,stripe}$ and $T_{theo,film}$, and the power of the blue plot in this speed range is derived to be about 0.62 which is near to the theoretical value (0.667). While at 50–100 μm s^{-1} (monolayer regime), $T_{expe,stripe}$ is higher than the theoretical value ($T_{theo,film}$), and shows an inverse relationship with pulling speed. At low U (50–100 μm s^{-1}), the length of entrainment (Figure 2b, *U*3) is short, and not far away from the meniscus. Therefore, the convective flow in the meniscus and capillary force may transport some solute molecules into the entrainment, and cause the deviation from the theoretical value. At higher U ($\geq$ 200 μm s^{-1}), the entrainment is high enough above the solution, so the capillary force could not carry many solutes to the top of entrainment before its drying. Accordingly, the growth in this regime is mainly controlled by entrainment, and follows the Landau–Levich equation.

To understand more details about this growth behavior, we further investigate the influence of some factors including solvent evaporation rate, solution concentration, solvent selection on the growth behavior (for details, see in the Supporting Information sections 7–9). Generally, it is found that 1) a low evaporation rate results in thicker microstripes, and is necessary for the assembly of solute molecules into uniform microstripes at high pulling speed (Figure S6). 2) Low solution concentrations result in less solute in the entrainment, and therefore provide more time to assembly into uniform thin microstripes, whereas a high concentration is necessary for thick microstripes with the trade-off of thickness uniformity (Figures S7,S8). 3) A proper selection of solvent is necessary for the growth of microstripes (Figure S9).

In addition, the generality of such growth behavior for OSCs is tested. Two other molecules, 2,7-dihexyl-s-indaceno[1,2-b:5,6-b′]dithiophene-4,9-dione (DIDTD-C6) and *N*,*N*′-dioctyl-3,4,9,10-perylenedicarboximide (PTCDI-C8) are selected. DIDTD-C6 shows a growth behavior similar to that of DTBDT-C6 (Figures S10,S11), which demonstrates the generality of such growth behavior for some soluble OSCs. However, PTCDI-C8 yields only discontinuous dots under similar growth conditions, which means this growth behavior cannot be generalized for any soluble OSCs. The molecular structure of organic semiconductor affects the nucleation rate and self-assembly ability and therefore significantly influences the growth behavior. Until now, it is difficult to deduce what kind of molecular structure is suitable for such growth behavior.

The ultrathin microstripes with monolayer precision provide a feasible and elaborate system for investigating charge transport properties of OSC films with a thickness comparable to a real conductive channel in organic field-effect transistors (OFETs). Therefore, top-contacted transistors were fabricated (Figure 4a). The field-effect mobility at different layer numbers is displayed in Figure 4b, indicating

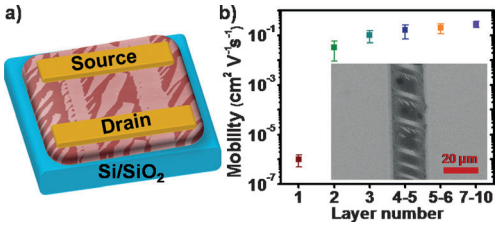

Figure 4. a) OFETs based on microstripes. b) Field-effect mobility of ultrathin microstripes with different layer numbers. The mobility range is obtained from 6–10 devices for each layer number. The inset shows a SEM image of the OFETs on microstripes.

that the mobility shows a slight increase when the layer number is above two, and almost saturates at four–six molecular layers. This finding is consistent with the basic operation principle of OFETs in which a real conductive channel is localized at the interface between semiconductor and insulator, and the first few molecular layers determine the electrical properties of the OFETs. In fact the charge transport property of ultrathin OSC films has been already reported.[4a,b,5a] However, in these reports the layer number is generally nominal or an average value because of nonuniform monolayer to multilayer films. Based on those systems, the effect of grain boundaries or partial multilayer coverage could not be eliminated. The continuity and uniformity of microstripes grown in this work can avoid such problems, and provide the possibility to reveal the intrinsic charge-transporting characteristics of OSCs. In addition, we have successfully fabricated high-performance gas ammonia OFET-based sensors with ultrathin microstripes, which benefit from efficient interaction between the conductive channel and analyte.[10] These results further prove the significance of uniform ultrathin microstripes for organic electronics.

In summary we demonstrate the monolayer precision growth of dendritic OSCs microstripes in nanometer thickness range via a dip-coating process. The pulling speed exerts pronounced influence on the layer number as well as the

thickness uniformity. The inverse (in the low-speed regime) and proportional (in the high-speed regime) *N*–*U* relationship is controlled by the meniscus and entrainment, respectively. Remarkably, in the high-speed regime a uniform monolayer to hexalayer microstripes with perfect monolayer precision can be obtained over a large area. This study provides a concept for the growth of organic semiconductor films with four distinguished features including nanometer thickness, monolayer thickness control precision, thickness uniformity (from monolayer to hexalayer) over large area, and microstructuring with 1D continuity. Such a precise growth represents a great progress for the assembly/growth of OSCs and is significant for both fundamental research and practical applications in organic and molecular electronics.

Experimental Section

Growth and characterization of ultrathin microstripes: 2,7-Dihexyldithieno[2,3-*d*;2′,3′-*d*′]benzo[1,2-*b*;4,5-b′]dithiophene (DTBDT-C6) was synthesized according to literature[11] and dissolved in toluene (Aldrich 99%, anhydrous). The silicon wafer with a 300 nm oxide layer (Si-Mat GmbH) was vertically immersed at 500 $\mu m s^{-1}$ into a solution and then pulled out of the solution at a speed ranging from 10 to 10000 $\mu m s^{-1}$. Dip-coating experiments were carried out at ambient temperature and pressure.

Device fabrication and characterization: The heavily doped silicon wafer and 300 nm thermally oxided SiO_2 layer was use as gate and insulator, respectively. Gold electrodes were deposited using a mask with a channel length of 20 μm. The channel width is calculated by the accumulation of each microstripe in the channel area. Field-effect characteristics measurements were performed on Keithley 4200 in air at room temperature. The field-effect parameters were obtained from the standard equation in the saturation region.

Received: August 7, 2013
Published online: October 31, 2013

Keywords: microstripes · molecular electronics · monolayers · organic semiconductors · self-assembly

[1] a) D. Görl, X. Zhang, F. Würthner, *Angew. Chem.* **2012**, *124*, 6434 – 6455; *Angew. Chem. Int. Ed.* **2012**, *51*, 6328 – 6348; b) H. Shao, J. Seifert, N. C. Romano, G. Min, J. J. Helmus, C. P. Jaroniec, D. A. Modarelli, J. R. Parquette, *Angew. Chem.* **2010**, *122*, 7854 – 7857; *Angew. Chem. Int. Ed.* **2010**, *49*, 7688 – 7691; c) Z. L. Wang, R. R. Bao, X. J. Zhang, X. M. Ou, C. S. Lee, J. C. Chang, X. H. Zhang, *Angew. Chem.* **2011**, *123*, 2863 – 2867; *Angew. Chem. Int. Ed.* **2011**, *50*, 2811 – 2815; d) K. Rahimi, I. Botiz, N. Stingelin, N. Kayunkid, M. Sommer, F. P. V. Koch, H. Nguyen, O. Coulembier, P. Dubois, M. Brinkmann, G. Reiter, *Angew. Chem.* **2012**, *124*, 11293 – 11297; *Angew. Chem. Int. Ed.* **2012**, *51*, 11131 – 11135; e) M. C. Yeh, Y. L. Su, M. C. Tzeng, C. W. Ong, T. Kajitani, H. Enozawa, M. Takata, Y. Koizumi, A. Saeki, S. Seki, T. Fukushima, *Angew. Chem.* **2013**, *125*, 1065 – 1068; *Angew. Chem. Int. Ed.* **2013**, *52*, 1031 – 1034; f) T. Osawa, T. Kajitani, D. Hashizume, H. Ohsumi, S. Sasaki, M. Takata, Y. Koizumi, A. Saeki, S. Seki, T. Fukushima, T. Aida, *Angew. Chem.* **2012**, *124*, 8114 – 8117; *Angew. Chem. Int. Ed.* **2012**, *51*, 7990 – 7993; g) L. Joon Seok, Y. Ilsun, K. Jangbae, H. Ihee, K. Bongsoo, P. Chan Beum, *Angew. Chem.* **2011**, *123*, 1196 – 1199; *Angew. Chem. Int. Ed.* ***2011***, ***50***, 1164 – 1167; h) D. Q. Liu, X. M. Xu, Y. R. Su, Z. K. He, J. B. Xu, Q. Miao, *Angew. Chem.* **2013**, *125*, 6342 – 6347; *Angew. Chem. Int. Ed.* **2013**, *52*, 6222 – 6227; i) L. Q. Li, L. Jiang, W. C. Wang, C. Du, H. Fuchs, W. P. Hu, L. F. Chi, *Adv. Mater.* **2012**, *24*, 2159 – 2164.

[2] a) J.-P. Hong, L. Seonghoon, *Angew. Chem.* **2009**, *121*, 3142 – 3144; *Angew. Chem. Int. Ed.* **2009**, *48*, 3096 – 3098; b) K. Xiao, J. Tao, Z. W. Pan, A. A. Puretzky, I. N. Ivanov, S. J. Pennycook, D. B. Geohegan, *Angew. Chem.* **2007**, *119*, 2704 – 2708; *Angew. Chem. Int. Ed.* **2007**, *46*, 2650 – 2654; c) M.-Y. Yuen, V. A. L. Roy, L. Wei, S. C. F. Kui, G. S. M. Tong, S. Man-Ho, S. S. Y. Chui, M. Muccini, J. Q. Ning, S. Xu, C. Chi-Ming, *Angew. Chem.* **2008**, *120*, 10043 – 10047; *Angew. Chem. Int. Ed.* **2008**, *47*, 9895 – 9899; d) J. E. Anthony, *Angew. Chem.* **2008**, *120*, 460 – 492; *Angew. Chem. Int. Ed.* **2008**, *47*, 452 – 483; e) A. Mishra, P. Bauerle, *Angew. Chem.* **2012**, *124*, 2060 – 2109; *Angew. Chem. Int. Ed.* **2012**, *51*, 2020 – 2067; f) S. S. Zade, M. Bendikov, *Angew. Chem.* **2010**, *122*, 4104 – 4107; *Angew. Chem. Int. Ed.* **2010**, *49*, 4012 – 4015; g) S. Allard, M. Forster, B. Souharce, H. Thiem, U. Scherf, *Angew. Chem.* **2008**, *120*, 4138 – 4167; *Angew. Chem. Int. Ed.* **2008**, *47*, 4070 – 4098; h) U. H. F. Bunz, J. U. Engelhart, B. D. Lindner, M. Schaffroth, *Angew. Chem.* **2013**, *125*, 3898 – 3910; *Angew. Chem. Int. Ed.* **2013**, *52*, 3810 – 3821; i) L. Q. Li, W. P. Hu, H. Fuchs, L. F. Chi, *Adv. Energy Mater.* **2011**, *1*, 188 – 193; j) A. Dadvand, A. G. Moiseev, K. Sawabe, W. H. Sun, B. Djukic, I. Chung, T. Takenobu, F. Rosei, D. F. Perepichka, *Angew. Chem.* **2012**, *124*, 3903 – 3907; *Angew. Chem. Int. Ed.* **2012**, *51*, 3837 – 3841.

[3] a) H. Usta, A. Facchetti, T. J. Marks, *Acc. Chem. Res.* **2011**, *44*, 501 – 510; b) H. Y. Li, B. C. K. Tee, J. J. Cha, Y. Cui, J. W. Chung, S. Y. Lee, Z. N. Bao, *J. Am. Chem. Soc.* **2012**, *134*, 2760 – 2765; c) A. M. Hiszpanski, S. S. Lee, H. Wang, A. R. Woll, C. Nuckolls, Y. L. Loo, *ACS Nano* **2013**, *7*, 294 – 300; d) H. Klauk, *Chem. Soc. Rev.* **2010**, *39*, 2643 – 2666; e) I. McCulloch, *Adv. Mater.* **2013**, *25*, 1811 – 1812; f) N. Stingelin-Stutzmann, E. Smits, H. Wondergem, C. Tanase, P. Blom, P. Smith, D. De Leeuw, *Nat. Mater.* **2005**, *4*, 601 – 606.

[4] a) F. Dinelli, M. Murgia, P. Levy, M. Cavallini, F. Biscarini, D. M. de Leeuw, *Phys. Rev. Lett.* **2004**, *92*, 116802; b) J. Huang, J. Sun, H. E. Katz, *Adv. Mater.* **2008**, *20*, 2567 – 2572; c) S. E. Fritz, S. M. Martin, C. D. Frisbie, M. D. Ward, M. F. Toney, *J. Am. Chem. Soc.* **2004**, *126*, 4084 – 4085; d) S. L. Ji, H. B. Wang, T. Wang, D. H. Yan, *Adv. Mater.* **2013**, *25*, 1755 – 1760; e) Y. Cao, Z. M. Wei, S. Liu, L. Gan, X. F. Guo, W. Xu, M. L. Steigerwald, Z. F. Liu, D. B. Zhu, *Angew. Chem.* **2010**, *122*, 6463 – 6467; *Angew. Chem. Int. Ed.* **2010**, *49*, 6319 – 6323; f) J. Yin, Z. Yan, L. Ting, P. Jian, *Angew. Chem.* **2011**, *123*, 6444 – 6447; *Angew. Chem. Int. Ed.* **2011**, *50*, 6320 – 6323; g) J. Lee, C. Hojong, K. Sangkwan, B. Gyeong Sook, L. Hyoyoung, *Angew. Chem.* **2009**, *121*, 8653 – 8656; *Angew. Chem. Int. Ed.* **2009**, *48*, 8501 – 8504; h) S. Fabiano, H. Yoshida, Z. H. Chen, A. Facchetti, M. A. Loi, *ACS Appl. Mater. Interfaces* **2013**, *5*, 4417 – 4422; i) L. Q. Li, M. H. Kopf, S. V. Gurevich, R. Friedrich, L. F. Chi, *Small* **2012**, *8*, 488 – 503; j) A. Hayoun Barak, G. de Ruiter, M. Lahav, S. Sharma, O. Gidron, G. Evmenenko, P. Dutta, M. Bendikov, M. E. van der Boom, *Chem. Eur. J.* **2013**, *19*, 8821 – 8831.

[5] a) S. Fabiano, C. Musumeci, Z. Chen, A. Scandurra, H. Wang, Y.-L. Loo, A. Facchetti, B. Pignataro, *Adv. Mater.* **2012**, *24*, 951 – 956; b) J. Matsui, Y. Sato, T. Mikayama, T. Miyashita, *Langmuir* **2007**, *23*, 8602 – 8606; c) J. Locklin, K. Shinbo, K. Onishi, F. Kaneko, Z. N. Bao, R. C. Advincula, *Chem. Mater.* **2003**, *15*, 1404 – 1412; d) L. Jiang, H. L. Dong, Q. Meng, H. X. Li, M. He, Z. M. Wei, Y. D. He, W. P. Hu, *Adv. Mater.* **2011**, *23*, 2059 – 2063; e) M. Defaux, F. Gholamrezaie, J. B. Wang, A. Kreyes, U. Ziener, D. V. Anokhin, D. A. Ivanov, A. Moser, A. Neuhold, I. Salzmann, R. Resel, D. M. de Leeuw, S. C. J. Meskers, M. Moeller, A. Mourran, *Adv. Mater.* **2012**, *24*, 973 – 978.

[6] L. Q. Li, P. Gao, K. C. Schuermann, S. Ostendorp, W. Wang, C. Du, Y. Lei, H. Fuchs, L. D. Cola, K. Müllen, L. Chi, *J. Am. Chem. Soc.* **2010**, *132*, 8807 – 8809.

[7] a) M. L. Le Berre, Y. Chen, D. Baigl, *Langmuir* **2009**, *25*, 2554 – 2557; b) M. Faustini, L. Benjamin, P. A. Albouy, M. Kuemmel, D. Grosso, *J. Phys. Chem. C* **2010**, *114*, 7637 – 7645; c) S. Roland, R. E. Prdu'homme, C. G. Bazuin, *ACS Macro Lett.* **2012**, *1*, 973 – 976.

[8] a) M. Ghosh, F. Fan, K. J. Stebe, *Langmuir* **2007**, *23*, 2180 – 2183; b) N. Liu, Y. Zhou, L. Wang, J. Peng, J. Wang, J. Pei, Y. Cao, *Langmuir* **2009**, *25*, 665 – 671; c) C. Zhang, X. Zhang, X. Zhang, X. Fan, J. Jie, J. C. Chang, C.-S. Lee, W. Zhang, S.-T. Lee, *Adv. Mater.* **2008**, *20*, 1716 – 1720; d) J. Huang, R. Fan, S. Connor, P. Yang, *Angew. Chem.* **2007**, *119*, 2466 – 2469; *Angew. Chem. Int. Ed.* **2007**, *46*, 2414 – 2417; e) J. Jang, S. Nam, K. Im, J. Hur, S. N. Cha, J. Kim, H. B. Son, H. Suh, M. A. Loth, J. E. Anthony, J.-J. Park, C. E. Park, J. M. Kim, K. Kim, *Adv. Funct. Mater.* **2012**, *22*, 1005 – 1014.

[9] a) L. Landau, B. Levich, *Acta Physicochim. URSS* **1942**, *17*, 42; b) J. W. Krozel, A. N. Palazoglu, R. L. Powell, *Chem. Eng. Sci.* **2000**, *55*, 3639 – 3650; c) M. Maleki, M. Reyssat, F. Restagno, D. Quéré, C. Clanet, *J. Colloid Interface Sci.* **2011**, *354*, 359 – 363.

[10] L. Q. Li, P. Gao, M. Baumgarten, K. Müllen, N. Lu, H. Fuchs, L. Chi, *Adv. Mater.* **2013**, *25*, 3419 – 3425.

[11] P. Gao, D. Beckmann, H. N. Tsao, X. Feng, V. Enkelmann, M. Baumgarten, W. Pisula, K. Müllen, *Adv. Mater.* **2009**, *21*, 213 – 218.

